

Joint estimation of afterslip rate and postseismic relaxation following the 1989 Loma Prieta earthquake

Fred F. Pollitz and Roland Bürgmann¹

Department of Geology, University of California, Davis

Paul Segall

Department of Geophysics, Stanford University, Stanford, California

Abstract. Global Positioning System (GPS) data from campaigns carried out over the 5 years following the 1989 Loma Prieta earthquake and leveling data measured in 1990 and 1992 define the postseismic velocity field around the Loma Prieta rupture zone. Subtraction of a background velocity field yields a residual velocity pattern which we interpret as the product of two physical processes: (1) slow afterslip along distinct planes in the upper crust and (2) viscoelastic relaxation of the lower crust and upper mantle. Bürgmann *et al.* [1997] previously derived an afterslip model involving uniform afterslip on two optimally determined planes, including oblique reverse slip on the coseismic rupture and reverse slip on a shallow thrust fault to the northeast of the San Andreas fault. We further consider models of distributed slip on these two fault planes plus a viscoelastic relaxation pattern which depends on a suitable coseismic rupture model and crust and mantle viscosities. Several fault models from the literature were considered for the 1989 coseismic rupture, with nearly identical impact on the results. Simultaneous maximum likelihood inversion of the GPS and leveling data for afterslip distribution and viscosity yields the following results: (1) A good fit to the data is obtained by smooth afterslip distributions without any viscoelastic relaxation being required. (2) Tangible broad-scale viscoelastic relaxation of the lower crust and upper mantle are present in this data set at 97% confidence, and a lower crustal viscosity of $\sim 10^{19}$ Pa s is obtained; however, the viscosity of both the lower crust and upper mantle are poorly constrained. (3) For a given misfit, 20% less integrated afterslip and smoother afterslip distributions result when viscoelastic relaxation is included. (4) Maximum slip rates on the slip-distributed models are 3–5 cm/yr, the dominant patches estimated on the two planes fill in the entire depth range 4–13 km without significant overlap, and deeper afterslip is not required. The afterslip distribution on the coseismic rupture plane is strongly dominated by reverse slip immediately southeast of the main center of coseismic reverse slip.

1. Introduction

Crustal deformation phenomena can, in simplified terms, be thought of as belonging to any of three categories: (1) interseismic strain accumulation [e.g., Savage, 1983], (2) coseismic deformation, which includes the main rupture and early aftershocks, often occurring on a single dominant rupture plane, and (3) postseismic deformation. The third category is generally divided into an afterslip phase, which involves "short-term" continued slip around the region of coseismic rupture, and a "long-term" relaxation phase, which involves some form of viscous relaxation of a ductile medium underlying the relatively shallow zone of earthquake generation. This picture (rather arbitrarily defined) suggests that afterslip is restricted to the brittle upper crust where elastic strain accumulation and release occur and that viscoelastic relaxation involves the lower

crust and upper mantle, where conditions are appropriate for ductile behavior of the constituent minerals [e.g., Brace and Kohlsteht, 1980; Chen and Molnar, 1983]. However, as demonstrated by Thatcher [1974, 1983], uniquely distinguishing between afterslip and viscoelastic relaxation mechanisms can be problematical under certain geometries, such as the case of strike-slip faulting on an infinitely long vertical fault [Savage and Prescott, 1978; Savage, 1990]. The case for one process or the other dominating in the years following an earthquake has been demonstrated for a few earthquakes. For example, afterslip concentrated along the coseismic rupture plane and its downdip extension dominates the deformation observed in the years following the 1923 Kanto, Japan, earthquake [Scholz and Kato, 1978], although the deeper afterslip inferred there is actually contrary to the sense of coseismic displacement. Afterslip along the downdip extension of the coseismic rupture plane (and in the same sense as the coseismic rupture) is inferred for earthquakes rupturing the Calaveras fault zone in 1979 and 1984 [Oppenheimer *et al.*, 1990], and over a period of weeks following the 1992 Landers earthquake [Shen *et al.*, 1994]. Deeper viscoelastic relaxation is the most plausible mechanism for persistent deformation observed far from the coseismic rupture zone following the 1894 Riku-U, earthquake, Japan

¹Now at Department of Geology and Geophysics, University of California, Berkeley.

[Thatcher *et al.*, 1980; Rydelek and Sacks, 1988, 1990]; the 1927 Tango earthquake, Japan [Tabei, 1989]; the 1975-81 Krafla rifting episode, Iceland [Foulger *et al.*, 1992; Pollitz and Sacks, 1996]; the 1857 Fort Tejon earthquake, California [Pollitz and Sacks, 1992]; and the 1906 San Francisco earthquake [Thatcher, 1983]. The decay times observed in these studies are typically 15 to 30 years. Very short decay times of the order of weeks or months have been derived from postseismic deformation data over relatively short time periods following the 1989 Loma Prieta earthquake [Linker and Rice, 1997] and the 1992 Landers earthquake [Shen *et al.*, 1994; Yu *et al.*, 1996], and this suggests some ambiguity in defining "afterslip" and "lower crustal relaxation" in the case when afterslip is inferred to occur below the seismogenic layer.

Some of the challenges currently facing crustal deformation analyses are to uniquely resolve the afterslip and viscoelastic relaxation phases, to determine the timescale and spatial scale appropriate for these deformation mechanisms, and to explore the implications for crust and mantle rheology. Detailed knowledge of the distribution of afterslip is potentially important for characterizing time-dependent stressing following earthquakes and characterizing the material properties of upper crustal fault zones. Improved constraints on the viscoelastic relaxation process in particular regions may lead to a means of distinguishing between power law and linear viscoelastic flow in the lower crust and mantle as well as better delineating the transfer of stress across fault zones in response to crustal stress release.

One well-studied region where a large amount of data may be brought to bear on these questions is northern California. The M7.1 Loma Prieta earthquake is one of the best studied earthquakes [e.g., Lisowski *et al.*, 1990; Kanamori and Satake, 1990; Romanowicz and Lyon-Caen, 1990; Ruff and Tichelaar, 1990; Marshall *et al.*, 1991; Snay *et al.*, 1991; Wald *et al.*, 1991; Wallace *et al.*, 1991; Williams *et al.*, 1993; Arnadottir and Segall, 1994], and the region affected by it has been monitored densely in space and time since 1989. The first detailed analysis of the postseismic deformation field [Savage *et al.*, 1994] examined 3 years of postseismic horizontal velocity data and showed that a model of deep afterslip combined possibly with fault zone collapse at depth were strong candidate processes for explaining the postseismic deformation. More recent analysis [Bürgmann *et al.*, 1997; hereafter referred to as paper 1] reveals that continued afterslip on the coseismic rupture plane and its extensions dominates the regional crustal deformation observed in the 5 years since 1989 as obtained by GPS measurements and leveling. Using the constrained nonlinear optimization algorithm of Arnadottir and Segall [1994], their analysis shows that uniform afterslip (predominantly reverse) on two distinct planes at rates of 1–3 cm/yr is sufficient to explain the primary features in the data. Our goal in this paper is to examine the same data set in greater detail by further considering: (1) distributed slip on the two afterslip planes determined by paper 1 and (2) viscoelastic relaxation of a lower crustal and mantle asthenosphere underlying the northern California upper crust. Assuming a Maxwell rheology for the mantle and a Maxwell or standard linear solid rheology [Cohen, 1982] for the lower crust, we shall obtain estimates of the distribution of afterslip velocity and viscosity through maximum likelihood inversion of the data. Our analysis will indicate where the estimates of afterslip are poorly constrained owing to the data distribution and will verify that afterslip, and not viscoelastic relaxation, is the dominant mechanism of deforma-

tion around the Loma Prieta rupture zone from 1989 to 1994. Nevertheless, a significant component of viscoelastic relaxation appears present in the data, and we shall indicate a range of viscosity models which are consistent with the observations.

2. Data Set

We employ 54 observations of horizontal Global Positioning System (GPS) velocity for the period 1989-1994 and 46 accumulated section height differences obtained along a leveling route for the period February/March 1990 to November 1992. These data are presented in Figures 4 and 6 of paper 1, respectively. In order to isolate the postseismic signal, the horizontal velocities must be corrected for the expected interseismic deformation. The latter has been estimated from pre-1989 trilateration data combined with GPS data in paper 1. Figure 1 shows the result of correcting the observed horizontal velocity field for the interseismic deformation. Although some spatial interpolation has been necessary to perform this correction, the smoothness of the background velocity pattern (Figure 8 of paper 1) suggests that little error is involved in this correction. The leveling data were collected along a line of benchmarks shown in Figure 6b, running roughly from southwest to northeast for a 56 km distance and crossing the main region of coseismic defor-

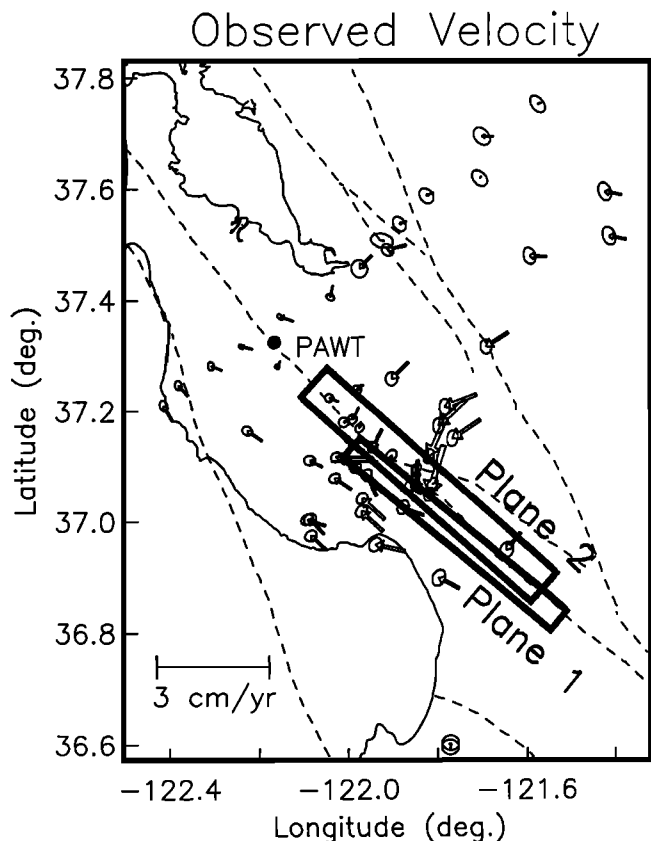


Figure 1. Residual velocity field computed from GPS data collected between October 19, 1989 and May 31, 1994. Velocities and their 1σ confidence ellipses are shown relative to fixed station PAWT. These residual velocities were determined by subtracting a background velocity pattern (pre-1989) from the observed velocities for the same 5-year period. Surface projections of fault planes 1 and 2 superimposed. Each of these faults dips toward the southwest. The complete fault geometry is defined in Table 1. After Bürgmann *et al.* [1997].

mation. The horizontal and vertical data and covariance information used here are identical to those employed in paper 1, except that the data covariance matrices are modified to have a component of nonmeasurement error as discussed below. paper 1 gives a detailed discussion of the GPS and leveling campaigns, repeatability of the measurements, and stability of the monuments.

3. Modeling Considerations

Paper 1 examined several candidate processes to explain the residual horizontal velocity pattern and vertical velocity pattern. Earlier proposed models involve either relaxation of the deeper extension of the coseismic rupture plane [Linker and Rice, 1997] or the imposition of oblique afterslip on the downdip extension combined with fault zone collapse [Savage et al., 1994]. The latter model well predicts the observed horizontal postseismic motions but significantly mispredicts the vertical motions. As described in paper 1, localization of the postseismic deformation near the rupture zone indicates shallow deformation sources. A single dislocation surface fails to fit the data, however, and the preferred model employed two dislocation surfaces. The simplest model which explains a large part of the signal in the data is the two-fault model of paper 1. Referring to Figure 1, this model consists of uniform afterslip on two distinct fault planes, one effectively coinciding with the coseismic rupture plane and dipping 70° toward the southwest, the other being a shallowly dipping extension of this plane towards the surface. We shall refer to these planes in this paper as plane 1 and plane 2, respectively. Despite the near-coincidence of plane 1 with the coseismic rupture plane, there is substantial formal uncertainty in the precise locations of planes 1 and 2. The afterslip rates on these planes were determined to be 1.7 cm/yr reverse and 1.8 cm/yr right-lateral strike-slip (plane 1) and 2.5 cm/yr reverse slip (plane 2). Arguments supporting the existence of plane 2 and its afterslip rate are the resulting good fit to both the leveling data as well as the pronounced large horizontal displacements perpendicular to the trend of the major faults in the region and its clear association with young surface topography and reverse aftershocks along its updip extension.

Further investigation into modeling this data set is motivated by the fact that viscoelastic relaxation of deeper ductile material is expected to have a strong strike-slip component in the sense observed. In addition, spatially distributed slip models for the 1989 coseismic rupture [e.g., Beroza, 1991; Amadottir and Segall, 1994] have identified areas which likely accommodated relatively large/small amounts of dip-slip and strike-slip motion. A distributed afterslip model for the postseismic phase could be interpreted in combination with a distributed slip model for the coseismic rupture to reveal spatial variability in the frictional

behavior of the fault planes being considered and to reveal the extent of local "slip deficit" which remained after the coseismic rupture. From the broadness of the aftershock distribution northeast of the coseismic rupture [Dietz and Ellsworth, 1990] and the geologic complexity of the local bend in the San Andreas fault [Jachens and Griscorn, 1998], it should also be considered that afterslip on additional thrust faults to the east of the Loma Prieta rupture zone could contribute to the postseismic velocity field observed at the surface. We did investigate the possible role of additional fault planes and found that a significant portion of the unexplained subsidence in the leveling data (paper 1) could be accounted for. Since this additional afterslip is much smaller than that already inferred in paper 1 for planes 1 and 2, it has little impact on the distributed afterslip models considered here, and we feel justified in neglecting it in the interest of simplicity.

The physical processes considered here are then: (1) distributed afterslip on planes 1 and 2 and (2) relaxation of the crust and upper mantle driven by the coseismic stress changes produced by the 1989 Loma Prieta earthquake. Parameters defining the afterslip planes are given in Table 1. In the slip models to be derived here, slip on plane 1 is allowed to have variable rake, while that on plane 2 is assumed to be purely reverse. The location of these afterslip planes projected along the strike of the San Andreas fault is shown in Figure 13 of paper 1 together with the post-1989 seismicity.

Calculation of the relaxation component of deformation requires the specification of a layered elastic-viscoelastic Earth model as well as a model for the coseismic rupture of the 1989 earthquake. We adopt the rheological model shown in Figure 2, consisting of a purely elastic upper crust underlain by a viscoelastic lower crust and mantle. The associated viscosities are denoted by η_c and η_m , respectively. Nearly all postseismic relaxation models considered will assume a Maxwell rheology for both regions; a standard linear solid rheology [Cohen, 1982] with long-term rigidity equal to one third of the short-term rigidity will be further considered for the lower crust. Since postseismic relaxation fields are generally long wavelength, with the thickness of the elastic upper layer acting as a long-wavelength filter, it suffices to consider a coseismic model for the 1989 earthquake with relatively few parameters. We considered the uniform slip models of several investigations [Lisowski et al., 1990; Marshall et al., 1991; Snay et al., 1991; Williams et al., 1993] and found very similar spatial patterns of relaxation resulting from all of these models, in spite of the somewhat different dips of the specified faults. Based on this and the desire to acknowledge the main result of the distributed slip inversions that coseismic reverse slip occurred primarily on the northwest portion of the coseismic rupture plane, we adopted the "two-plane" model of Marshall et al. [1991]. This particu-

Table 1. Afterslip Fault Geometry

Plane	Strike ^a	Dip, deg	Rake ^b	Length, km	Fault lat, ° N	Endpoint ^c lon, ° E	Bottom Depth, km	Top Depth, km
1	130	70	---	53.82	36.80	-121.55	15.57	1.48
2	132	30	90	61.40	36.86	-121.59	6.11	1.62

^aDegrees clockwise from North.

^bSlip direction of hanging wall measured in degrees counterclockwise from strike direction (90° is pure reverse slip).

^cLowermost corner of fault closest to strike direction.

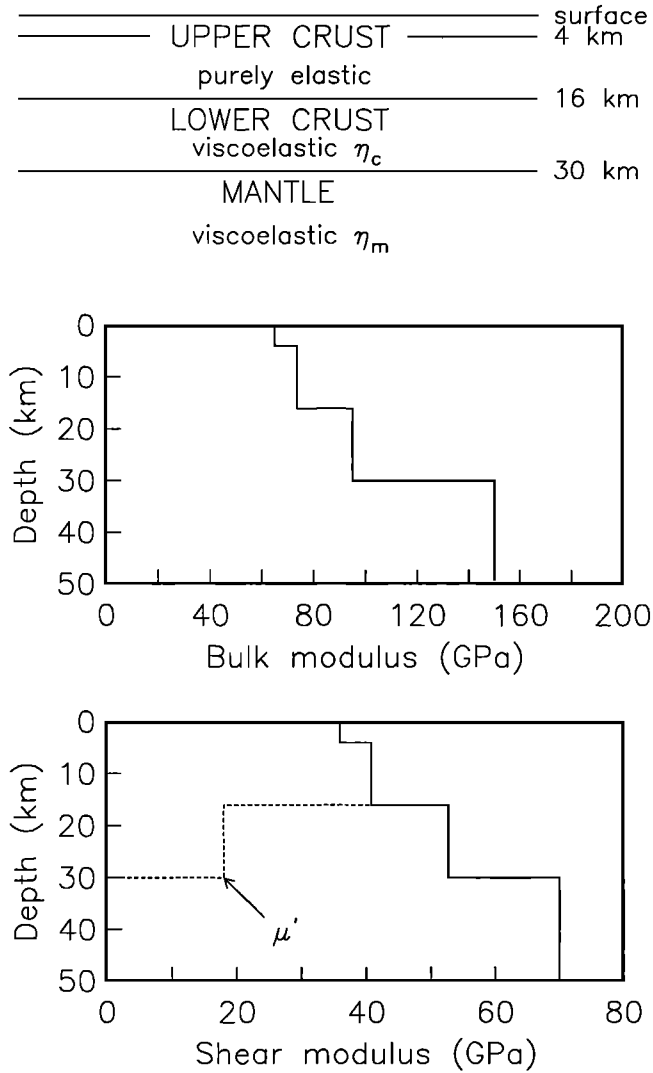


Figure 2. Elastic and viscosity parameters of the San Francisco Bay area crust and upper mantle used in this study. The stratification in elastic parameters is consistent with the range of one-dimensional crustal structure models summarized by *Blümling et al.* [1985].

lar fault model involves a combination of right-lateral strike-slip and reverse components on two connected fault planes dipping 62° toward the southwest. For specified η_c and η_m , the calculation of viscoelastic relaxation effects is then done using the method of *Pollitz* [1992] with modification for a standard linear solid rheology as outlined by *Pollitz and Sacks* [1996]. This method yields the time-dependent postseismic deformation on a layered elastic-viscoelastic model for a point source of deformation in an elastic layer, and finite sources are realized by numerical integration of point sources along a fault plane.

An example of postseismic relaxation accumulated over the period 1989-1994 for a particular viscosity combination is shown in Figure 3. Each displacement field is decomposed into its two post-strike-slip and post-reverse-slip components (one set for each of the two fault planes in the two-fault model of *Marshall et al.*, [1991], with the total displacement field shown in the upper left part of the figure. It is noteworthy that the center of symmetry for the post-thrusting components is located updip of the fault planes, while the center of symmetry for the

post-strike-slip components is located at the surface projection of the downdip extension of the fault planes. Maximum postseismic velocities are concentrated near the rupture zone and reach about 2 mm/yr for both the horizontal and vertical components.

The time dependence of postseismic velocity has been analyzed by *Savage et al.* [1994] and *Segall and Bürgmann* [1997]. *Savage et al.* [1994] identified exponentially decaying behavior in fault-normal displacement components with a time constant of about 1.4 years, but no clear exponentially decaying behavior in the fault-parallel components. Since forward models of postseismic relaxation generally yield greater relaxation in the fault-parallel sense than the fault-normal sense (Figure 3), any resolvable signal due to postseismic relaxation would exhibit exponentially decaying behavior in at least the fault-parallel component. Therefore we interpret both the spatial pattern and the time constant found by them as primarily attributes of the afterslip-generated velocity field. This agrees with the time-dependent filter analysis of *Segall and Bürgmann* [1997], who find considerable spatial and temporal complexity in the afterslip rate distributions necessary to explain the time-dependent data. In this paper we seek to identify a longer-duration temporal signal (postseismic relaxation) in the presence of a large afterslip signal and to understand the first-order trade-offs between the two processes. Therefore we shall not attempt to model variations in postseismic velocity over the period 1989-1994 but only the average velocity.

4. Inversion

The amount of data (54 horizontal velocity vectors and 46 accumulated vertical section differences) and their distribution have the potential to define details of the afterslip pattern with good spatial resolution. For those fault planes where we seek distributed afterslip, it is convenient to parameterize the local

$$v(x,y) = c_{-1-1} + \sum_{l=0}^{l_{\max}} \sum_m c_{lm} h_l\left(\frac{x}{L_1}\right) h_m\left(\frac{y}{L_2}\right) \times \exp\left[-\frac{x^2}{2L_1^2} - \frac{y^2}{2L_2^2}\right] \quad (1)$$

where the fault plane is taken to be a rectangle on the x - y plane. The h_l are normalized Hermite polynomials of order l [*Abramowitz and Stegun*, 1964] such that

$$\int_{-\infty}^{\infty} h_l(x) h_m(x) e^{-x^2} dx = \delta_{lm} \quad (2)$$

The term c_{-1-1} represents spatially uniform slip rate along the entire fault plane. The summation in (1) is performed over those pairs (l,m) such that $l+m \leq l_{\max}$. Hermite-Gaussian functions of this form were introduced by *Friederich and Wielandt* [1995] to parameterize the phase velocity distribution of seismic surface waves. They have the advantage of being spatially bounded on the x - y plane, and through the scaling parameters L_1 and L_2 , it is easy to control their spatial extent. Such a parameterization can be used for both the reverse and strike-slip components of afterslip rate.

Inversion of the data yielding a maximum likelihood solution is performed by minimizing a penalty function of the form

$$\beta^2 = \chi^2 + \mu \sum_j \langle |\nabla v_j(x,y)|^2 \rangle \quad (3)$$

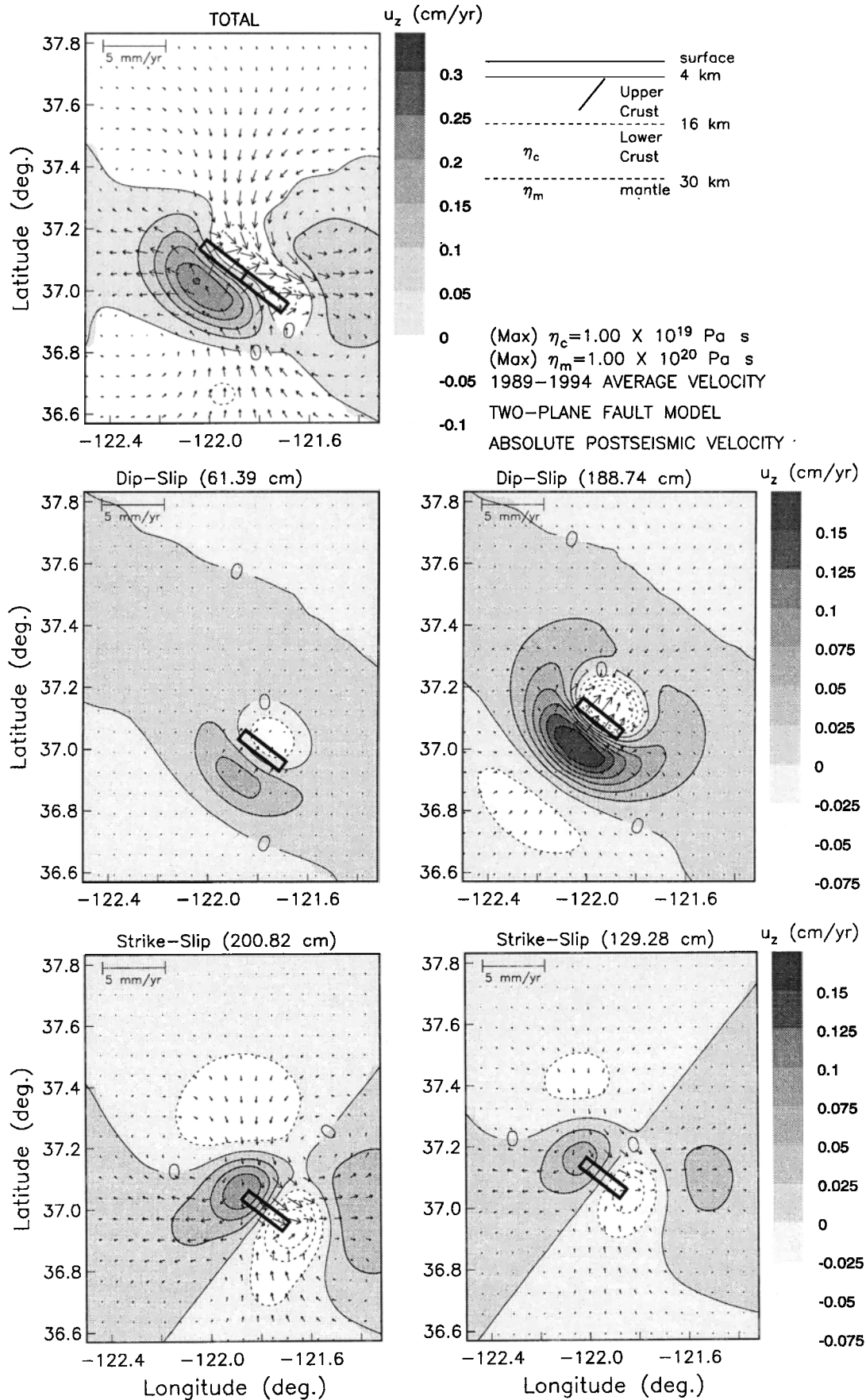


Figure 3. Synthetic horizontal and vertical postseismic velocity from 1989 to 1994 from relaxation of the "two-plane" Loma Prieta coseismic rupture model of *Marshall et al.* [1991]. The viscoelastic relaxation is calculated for the viscosity combination $\eta_c = 1 \times 10^{19}$ Pa s and $\eta_m = 1 \times 10^{20}$ Pa s. Postseismic relaxation patterns are calculated separately for the coseismic reverse and right-lateral strike-slip components on each of two adjacent fault planes. The sum of these four components is shown at the top left part.

where

$$\tilde{\nabla} = \frac{L_1}{\sqrt{L_1^2 + L_2^2}} \frac{\partial}{\partial x} \hat{x} + \frac{L_2}{\sqrt{L_1^2 + L_2^2}} \frac{\partial}{\partial y} \hat{y} \quad (4)$$

$$\chi^2 = (\mathbf{d}_H^{\text{obs}} - \mathbf{G}_H \mathbf{m})^T \mathbf{C}_H^{-1} (\mathbf{d}_H^{\text{obs}} - \mathbf{G}_H \mathbf{m}) + (\mathbf{d}_V^{\text{obs}} - \mathbf{G}_V \mathbf{m})^T \mathbf{C}_V^{-1} (\mathbf{d}_V^{\text{obs}} - \mathbf{G}_V \mathbf{m}) \quad (5)$$

The second term in equation (3) penalizes the weighted roughness of the afterslip distributions averaged over the areas of the respective fault planes. The summation over j for this term is for all slip planes and slip senses. Uniform slip distributions through the term c_{-1-1} do not contribute to the roughness. The contribution of roughness to the penalty function is calculated in terms of the expansion coefficients $\{c_{lm}\}$ through the fourth term of equation (21) of *Friederich and Wielandt* [1995]. The spatial scales L_1 and L_2 for each fault plane are chosen to be proportional to the fault length and width, respectively, such that the last maximum of the highest-order Hermite-Gaussian function is located on the edge of the fault plane. Assuming locally linear dependence of postseismic relaxation fields on η_c , minimization of (3) then becomes a linear inversion for the parameters described above. Iteration of this process rapidly reduces the nonlinear dependence of the forward problem on η_c and yields final estimates of the afterslip distribution parameters and viscosities.

The notations H and V in (5) refer to the horizontal and vertical data, respectively, \mathbf{d} is the observed data, \mathbf{C} is the data covariance matrix, and \mathbf{G} are Green's functions for afterslip distribution, viscosity, and a rigid translation of all position data (since both the horizontal and vertical data are defined with respect to fixed reference points). The Green's functions for afterslip rate are prescribed by the formulas for coseismic deformation on a layered spherical Earth by *Pollitz* [1996]. In inversions which include viscoelastic relaxation effects, the ratio η_c/η_m is held fixed and an iterative nonlinear inversion for η_c is performed. The model vector \mathbf{m} contains the set of coefficients $\{c_{lm}\}$ (one set for every afterslip plane and slip sense), η_c , and three additional parameters for translation. With $l_{\text{max}} = 14$, this yields 242 parameters for the combined strike-slip and reverse afterslip distributions on plane 1, 121 parameters for the reverse afterslip distribution on plane 2, plus four additional parameters, adding up to a total of 367 parameters.

The data covariance matrices have the form

$$\mathbf{C}_H = \mathbf{C}_H^0 + \epsilon_H^2 \mathbf{I} \quad (6)$$

$$\mathbf{C}_V = \mathbf{C}_V^0 + \epsilon_V^2 \mathbf{I} \quad (7)$$

where \mathbf{I} is the identity matrix and superscript 0 denotes that component of the data covariance matrix arising from measurement errors only. \mathbf{C}_H^0 includes the formal errors of the coordinates determined using the Bernese GPS analysis software, scaled by a constant factor. These are then used together with the covariance of the preseismic model predictions to determine the final covariance matrix of the postseismic residual velocities relative to the reference station. The second term in (6) allows for a degree of nonmeasurement error in the horizontal GPS measurements, which may include the effect of random walk errors due to local ground instability or unmodeled deformation processes. Since all of the GPS sites are located in relatively stable hard rock, we have chosen a small value $\epsilon_H = 0.04$ cm/yr. For a 5-year observation period, this is equivalent to an average random walk error of 0.9 mm/ $\sqrt{\text{yr}}$, which is slightly

smaller than the average random walk errors obtained by *Langbein and Johnson* [1997]. For the leveling data, \mathbf{C}_V^0 is specified by *Arnadottir et al.* (1992) in a form which is equivalent to treating the section height differences as having independent, identically distributed random components. Thus, by employing \mathbf{C}_V^0 for the leveling data we are essentially fitting the slope of the observed leveling curve. While from a statistical point of view this is correct, attention must be paid to possible leveling monument instability, which can lead to large excursions in a few of the section height differences, particularly (as in the present case) when the monuments are closely spaced. Since the model space can accommodate only relatively smooth changes in the accumulated section height differences, monument instability (due to such factors as unmodeled local faulting and ground water migration) can lead to data residuals which are not Gaussian distributed. For this reason, we have introduced the second term on the right-hand side of equation (7), which is designed to account for nonmeasurement errors in the accumulated section height differences which are assumed to be uncorrelated with the measurement error. In several inversion trials it was noted that when this second term was ignored, results appeared biased toward fitting a few locally extreme values of the slope of the leveling curve at the expense of smoother trends in both the leveling and GPS data, which should be the more robust features of the signal. By taking a root-mean-square nonmeasurement noise level of $\epsilon_V = 0.05$ cm/yr, a value which is consistent with the long-period noise levels in vertical motion obtained by *Wyatt* [1989], this tendency for bias is sharply reduced, and the robust features of the data then have the appropriate influence on the model estimation. We note that because each of the leveling benchmarks, including the reference benchmark, now has a formal uncertainty in its respective absolute height, one additional parameter (vertical translation) has been introduced into the inversion in order to account for the slightly uncertain reference level.

In order to test this procedure, synthetic afterslip rate distributions in the form of Gaussian slip patterns were generated, synthetic horizontal and section difference data with the actual geographic data distribution and covariance structure were calculated and then treated exactly as the real data in the inversion process. The damping parameter μ was chosen to be that employed in the best inversion of the real data, as discussed below. Figure 4 shows the results of six such tests. In each test, synthetic reverse slip on patches of either reverse (Figure 4a) or strike-slip (Figure 4b) sense on plane 1 were specified together with an input crustal viscosity η_c , indicated in the top left subplot of each panel. The mantle was taken to be purely elastic in these simulations ($\eta_c/\eta_m = 0$). The estimated slip distributions on planes 1 and 2 and estimated η_c are given in each panel. It is noteworthy that reverse slip distributions localized on the northwest portion of plane 1 can be recovered well by the inversion, whereas possible slip occurring on the southeast portion of this plane can not be resolved. Qualitatively similar results are obtained for an input reverse afterslip signal on plane 2. These results clearly reflect the data distribution, which is most sensitive to afterslip on the northwest portions of these fault planes. In all cases, few artifacts are introduced into the afterslip fields (for example, small inverted afterslip in the strike-slip sense on plane 1 for input reverse afterslip). Crustal viscosity η_c is also well estimated in all cases. Although the maximum input slip value is always underestimated by the inverted slip distributions, the area-integrated

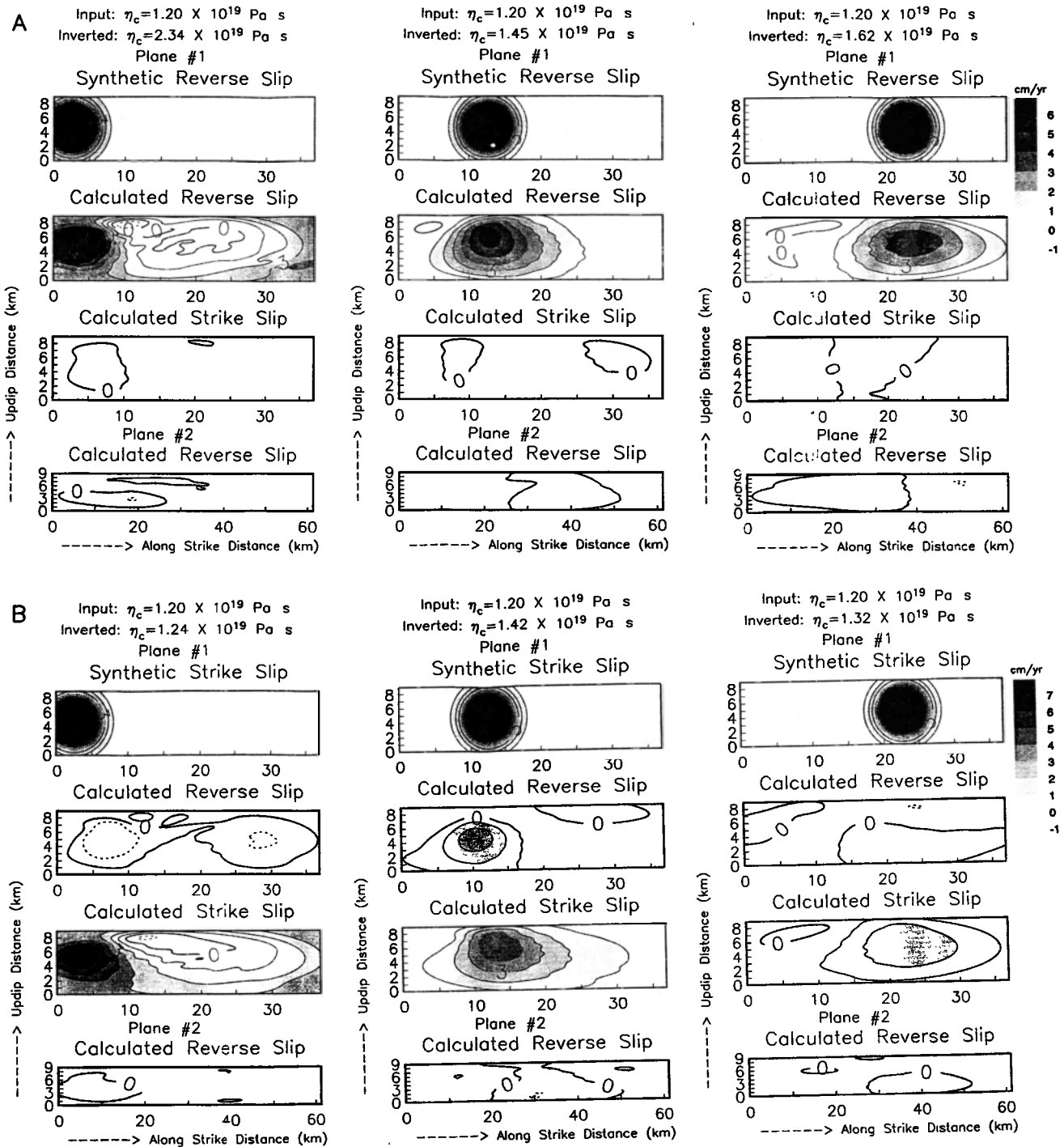


Figure 4. Synthetic velocity vectors and uplift rates are generated for synthetic distribution of slip on plane 1, including the effects of postseismic relaxation with a lower crustal viscosity of 1.2×10^{19} Pa s and a purely elastic mantle. The synthetic data are inverted in exactly the same manner as the data, using the same damping parameter μ as used in deriving model A with the real data. Results are shown for several Gaussian input afterslip signals of either (a) reverse or (b) right-lateral strike-slip sense on plane 1.

inverted slip distributions are very close to those of the corresponding input slip distributions.

5. Results

The details of several models obtained by inversion of the data are listed in Table 2. Where viscoelastic relaxation is

included, the elastic plate thickness and estimated viscosities are listed. For all models, the total roughness (the sum which appears in equation (3)), vertical and horizontal χ^2 (two terms in equation (5)) and their sum are listed.

Among all of the models, we consider model A to provide the best fit to the data with a relatively small level of roughness. This model represents the San Francisco Bay area crust and upper mantle in terms of a 16-km-thick elastic upper crust

Table 2. Inversion Results

Model	H_e^a , km	Viscosity ^b , $\times 10^{19}$ Pa s	Planes 1+2 Total Roughness	χ_v^2	χ_h^2	χ^2^c Total
A	16	(Max) $\eta_c = 1.4$ $\eta_m = \infty$	4.04	114.6	287.7	402.3
B	20	(Max) $\eta_c = 2.7$ $\eta_m = \infty$	4.04	114.6	302.9	417.5
C	16	(Sls) $\eta_c = 2.9$ (Max) $\eta_m = 0.86$	4.04	114.1	291.3	405.5
D	--	none	4.04	113.5	309.2	422.7
E	--	none	6.75	107.9	294.4	402.3
F	--	none	0.00	176.9	438.5	615.5
F'	16	(Max) $\eta_c = 1.2$ $\eta_m = \infty$	0.00	175.7	407.2	582.9
G	16	(Max) $\eta_c = 0.87$ $\eta_m = \infty$	no afterslip	232.8	739.8	972.7
H ^d	16	none	4.43	186.2	467.4	653.6

H_e , elastic plate thickness; η_c , crustal viscosity; η_m , mantle viscosity.

^aAll inversions. H_e , ratio η_c/η_m are fixed.

^bMax, Maxwell viscoelastic solid; Sls, standard linear solid.

^cNULL MODEL. $\chi_v^2=236.1$, $\chi_h^2=1001.7$, and $\chi^2(\text{total})=1237.8$.

^dAfterslip and fault zone collapse on coseismic rupture plane.

underlain by a Maxwell viscoelastic lower crust with viscosity $\eta_c = 1.4 \times 10^{19}$ Pa s and a purely elastic upper mantle below 30 km depth, and it employs both distributed afterslip and postseismic viscoelastic relaxation simultaneously to fit the geodetic data. Model B is designed to accommodate the fact that San Francisco Bay area seismicity can extend deeper than 16 km [Dietz and Ellsworth, 1990; Seeber and Armbruster, 1990; Olson and Hill, 1991], suggesting that a thicker upper layer exhibiting purely elastic behavior might be a better representation for deeper semibrittle behavior. It also fits the data jointly with distributed afterslip and postseismic relaxation but yields a larger misfit for the same level of model roughness. With model C we again explore semibrittle behavior in the lower crust by representing it as a standard linear solid, and we further assume that the underlying upper mantle is weaker than the lower crust, a situation which appears to apply to north central Japan [Tabei, 1989] and northeast Iceland [Pollitz and Sacks, 1996]. As with models A and B, model C allows for both distributed afterslip and postseismic relaxation, and it does nearly as well as model A in fitting the geodetic data at a given level of misfit.

An important question is whether viscoelastic relaxation of the lower crust and upper mantle following the 1989 Loma Prieta earthquake is a viable physical process. This question is addressed by models A, B, and C (which allow for both distributed afterslip and postseismic relaxation) and models D and E (which allow for only distributed afterslip). Comparing models A, B, and C with model D in Table 2 shows that at a given level of misfit, the inclusion of relaxation significantly improves

the fit obtained with distributed afterslip only. To consider this further from the point of view of model roughness, the distributions of afterslip rate on models A and E are shown in Plate 1. Each of the models displayed has two views of the reverse afterslip rate distribution (one view has plane 1 removed to improve the display of plane 2) and one view of the strike-slip afterslip distribution. On model A, the maximum afterslip rates achieved on planes 1 and 2 are 3-5 cm/yr averaged over the 5-year observation period, and the regions of high afterslip rate fill in the entire depth interval 4-13 km with little overlap. These regions of locally high rates are correlated with a high rate of aftershock seismicity (Figure 13 of paper 1). Plate 1 also shows that greater afterslip roughness is required on a model without relaxation (model E) for the same level of total misfit as model A.

A comparison of the observed horizontal velocity patterns with the calculated velocity pattern for model A is shown in Figure 5. The lowermost subplot shows where model A was chosen on the trade-off curve between afterslip roughness and total χ^2 . It is clear that duplication of nearly every feature of the observed velocity pattern, particularly that component perpendicular to the San Andreas fault, is attained with model A. The relaxation component is plotted with a larger scale and exhibits a maximum horizontal velocity of about 0.15 cm/yr. A similar comparison of the observed and calculated uplift rate along the leveling profile is shown in Figure 6a for several of the models. Both the total calculated and the relaxation components are shown. It is clear that the relaxation component alone is poorly correlated with the observed leveling profile.

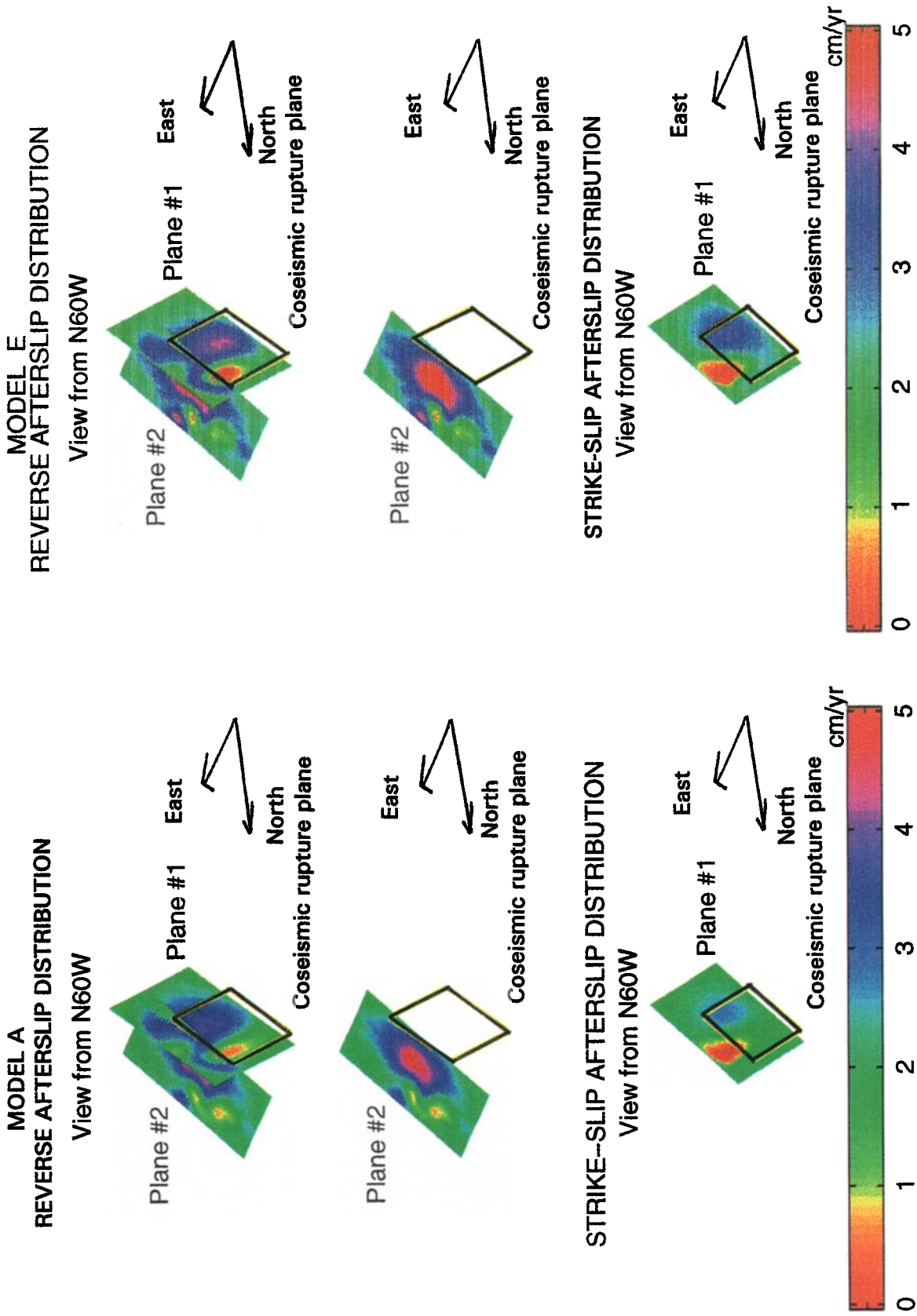


Plate 1. Three-dimensional view of reverse and right-lateral strike-slip afterslip distribution on the two fault planes in models A and E of Table 2. For each model, the reverse afterslip distribution is shown twice, the second time with plane 1 removed in order to better reveal plane 2. The coseismic rupture plane of *Williams et al.* [1993] is superimposed and projected slightly northwest of plane 1 to render it visible.

MODEL A

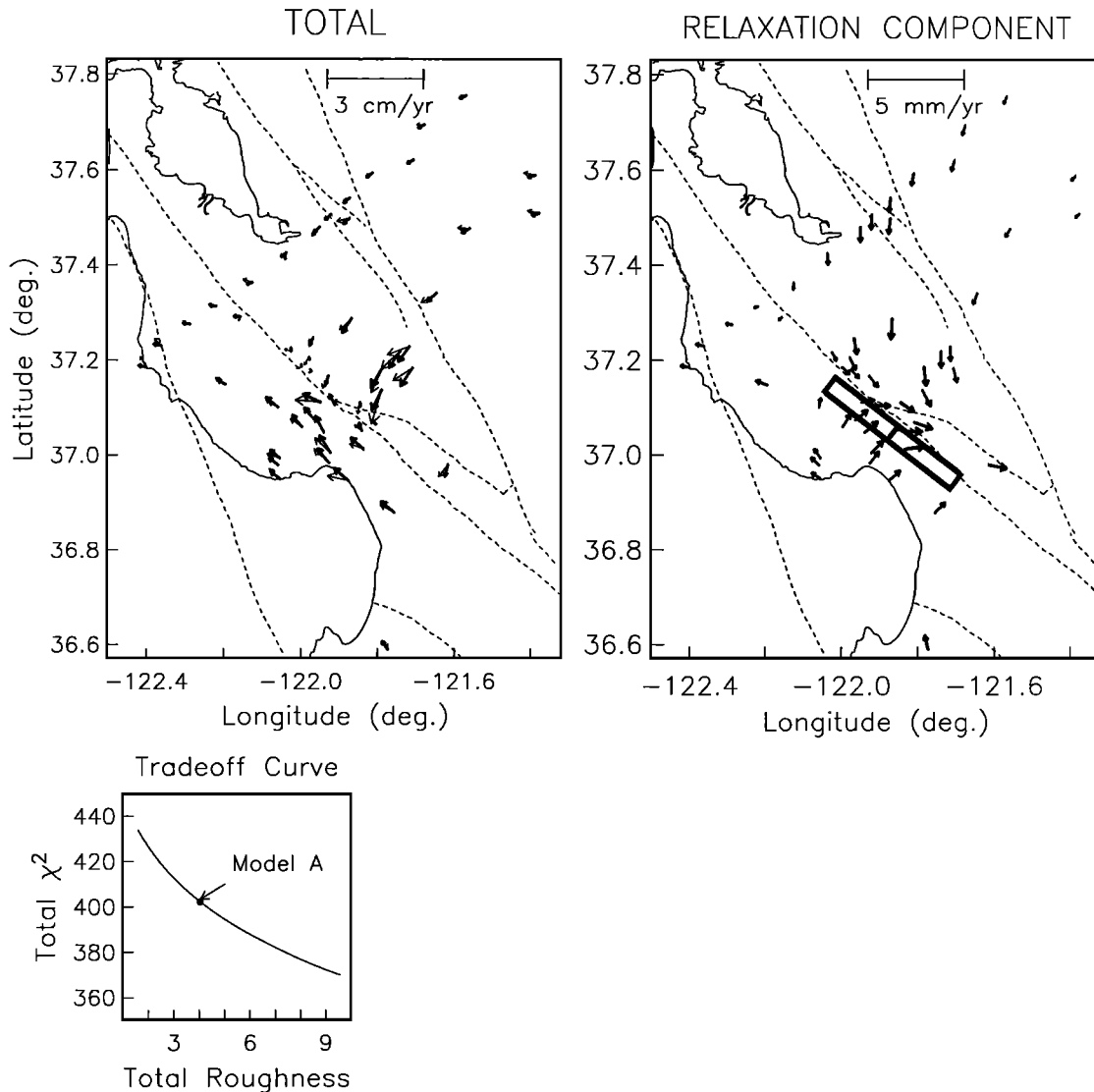


Figure 5. The observed (light solid arrows) and calculated (heavy solid arrows) horizontal velocity vectors on model A. The top left-hand plot shows the total afterslip plus relaxation plus translation components, and the top right-hand plot shows the relaxation component plotted at a larger scale.

Figure 6a also verifies our expectation that distributed afterslip models generally fit the leveling data better than a uniform afterslip model. For instance, we derived model F by modeling only uniform afterslip rate on planes 1 and 2. It is nearly identical to the two-plane model of paper 1, with only slight differences in the afterslip rate estimates due to the inclusion of the nonmeasurement error terms in (6)-(7); the slip estimates obtained in model F/paper 1 are 1.5/1.7 cm/yr (dip slip on plane 1), 2.0/1.8 cm/yr (right-lateral strike slip on plane 1), and 2.5/2.5 cm/yr (dip slip on plane 2). Comparing model F with the other four models shown in Figure 6a, the inclusion of distributed afterslip significantly improves the fit of leveling data obtained with uniform afterslip on planes 1 and 2 alone, and Table 2 shows that the same conclusion is also valid for the horizontal data.

An attempt to fit the data with a simple model of postseismic relaxation alone explains only about 20% of the variance

(model G in Table 2). The corresponding fit to the data is shown in Figure 7. Note that postseismic relaxation explains well that portion of the horizontal data characterized by right-lateral motion about a line parallel to the San Andreas fault but that the vertical data and fault-perpendicular motion are poorly explained by it. This result is similar to that obtained by *Linker and Rice [1997]*, who considered viscoelastic relaxation of the aseismic downdip extension of the coseismic fault plane. If the vertical data were removed as a constraint, then for the same elastic plate thickness and ratio η_c / η_m as used in model G, a χ^2 of 506.6 would be obtained with a model of postseismic relaxation alone, equivalent to a variance reduction of 49% with respect to the horizontal data. However, such a model appears incapable of explaining the observed large horizontal displacements perpendicular to the trend of the San Andreas fault (Figure 1), and the large afterslip rates derived here are necessary to account for that feature of the observa-

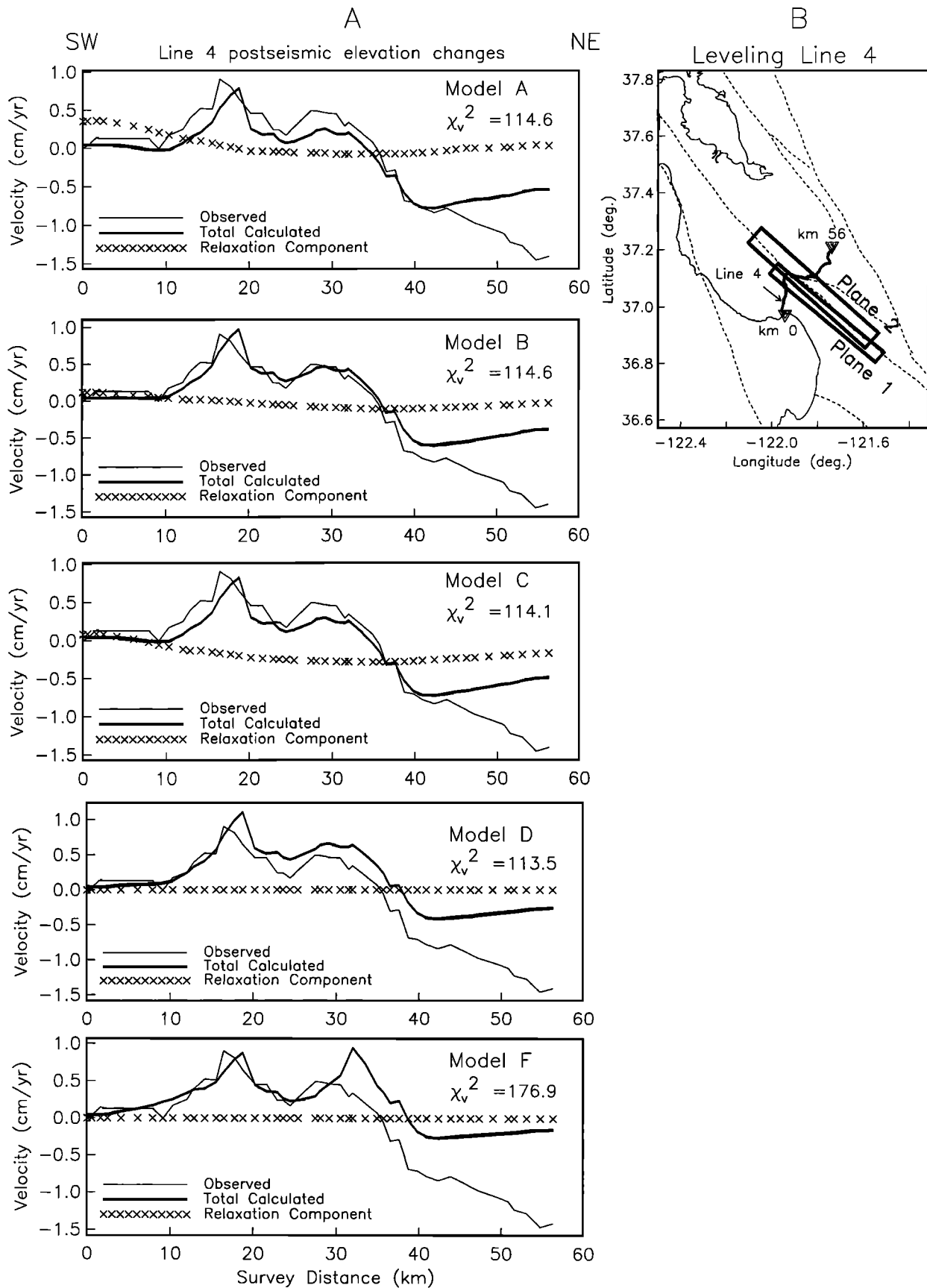


Figure 6. (a) Comparison of observed and calculated vertical uplift rates along the observed leveling profile for several different models. The total calculated leveling profiles are a sum of afterslip, relaxation, and vertical translation components. Models A, B, C, and D, each of which includes distributed afterslip, fit the leveling profile significantly better than model F, which utilizes only uniform afterslip on planes 1 and 2. (b) Location of leveling line [Marshall et al., 1991, Line 4].

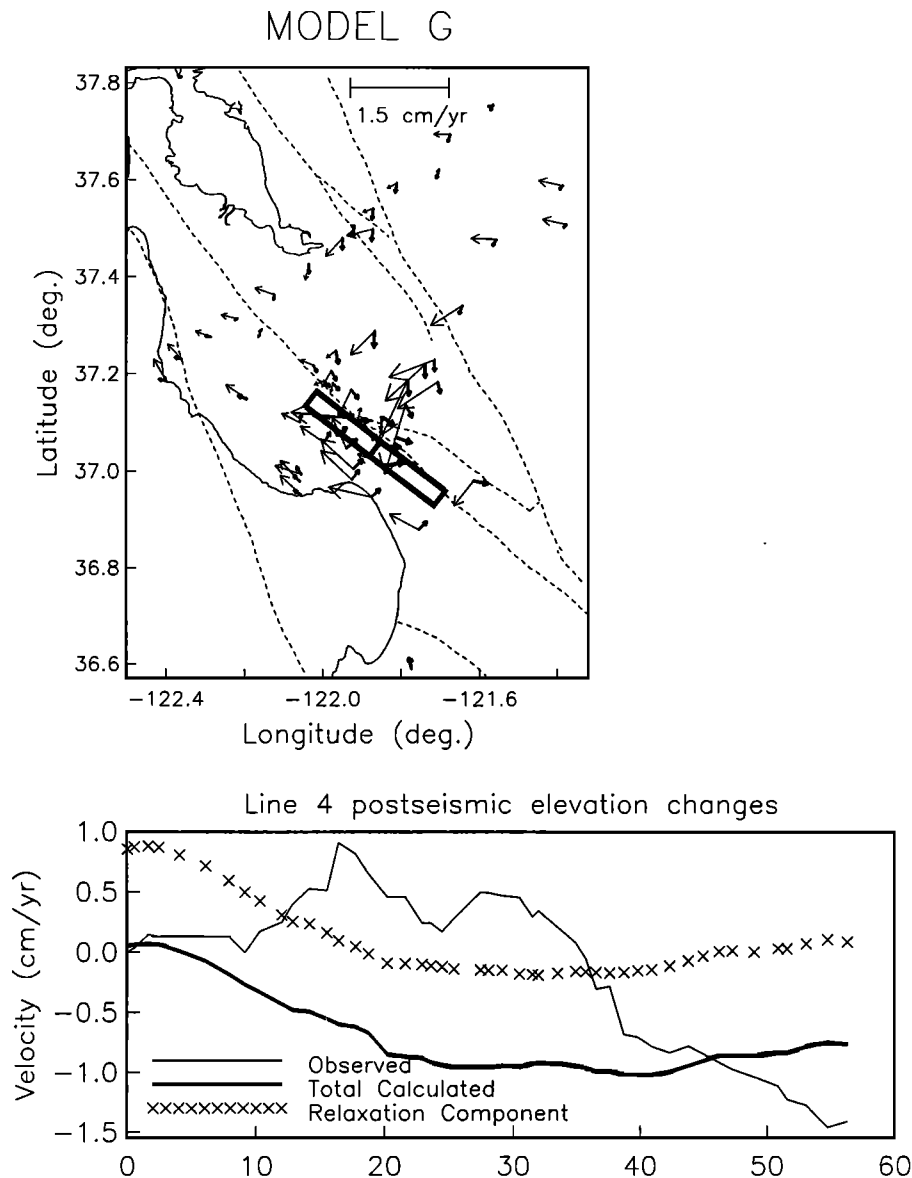


Figure 7. Comparison of observed horizontal and vertical velocities with the corresponding velocities calculated on model G (Table 2), which attempts to fit the data with postseismic relaxation only. The total calculated vector rates are a sum of relaxation and horizontal or vertical translation components (i.e., the total calculated leveling profile differs from the relaxation component by a constant across the profile). A variance reduction of 21% is achieved with model G. If the leveling profile were to be ignored, then a variance reduction of 49% for the horizontal velocity data could be achieved with a model of postseismic relaxation alone.

tions. Considering the appreciable strike-slip component of displacement generally associated with the postseismic relaxation fields considered here (Figure 5), there is obviously a trade-off between the size of the relaxation component and the amount of afterslip in the strike-slip sense which is required. Comparing models A and E in Plate 1, the amount of right-lateral afterslip required to fit the data is smaller when postseismic relaxation is included.

6. Discussion

Considering the class of distributed slip models, the impact of viscoelastic relaxation of the lower crust on the surface postseismic velocity field is bounded by model A, which includes

distributed afterslip and relaxation, and model D, which includes only distributed afterslip. From Table 2, we find that the improvement in total variance reduction resulting from inclusion of postseismic relaxation is $(422.7 - 402.3)/1237.8 = 1.7\%$. This is very small compared with the 66% variance reduction achieved with a model of distributed afterslip alone (model D) or with the 50% variance reduction achieved with a model of uniform afterslip (model F). Thus postseismic relaxation, even if it is a viable process during the years following the Loma Prieta earthquake, has contributed only a small signal during the first 5 years. In spite of the apparently low signal in the data, we can establish that the obtained relaxation component is highly significant by focussing on a simpler class of models, those in which uniform afterslip is assumed on the two

afterslip planes. In the absence of postseismic relaxation, the χ^2 from the uniform afterslip model is 615.5 (model F, which employs the optimally determined afterslip planes derived in paper 1). We find that introducing postseismic relaxation, assuming $\eta_c/\eta_m = 0$ (only lower crustal relaxation, as in model A), yields uniform afterslip rates of 1.4 cm/yr (dip slip on plane 1), 1.8 cm/yr (right-lateral strike slip on plane 1), and 2.2 cm/yr (dip slip on plane 2) and a residual χ^2 of 32.6 (model F' in Table 2). We obtain a reduction in χ^2 of 32.6 with model F' compared with model F, which is highly significant for an addition of only 2 degrees of freedom. This reduction in χ^2 may be evaluated with an F test. If $\chi^2(n)$ is the residual variance resulting after least squares fitting with n degrees of freedom and N is the number of independent data, then χ^2 follows the χ^2 distribution with $\nu = N - n$ degrees of freedom [Bevington, 1969, equation (10.4)]. If two more parameters are used in the least squares inversion, then the difference $\chi^2(n+2) - \chi^2(n)$ follows the χ^2 distribution with 2 degrees of freedom. Then the quantity

$$f = \frac{(\chi^2(n+2) - \chi^2(n)) / 2}{\chi^2(n+2) / (N - n - 2)} \quad (8)$$

is distributed according to the F distribution $P_f(f, 2, N-n-2)$ defined in equation (10.6) of Bevington [1969]. The probability that $f \geq F$ is

$$P_F(F, 2, N-n-2) = \int_F^{\infty} P_f(f, 2, N-n-2) df \quad (9)$$

In our application, $N = 2 \times 54$ (the number of horizontal vectors) + 47 (the number of leveling sites, including the reference site) = 155, $n = 3$ (dip-slip and strike-slip uniform afterslip rates on plane 1 plus dip-slip uniform afterslip rate on plane 2) + 3 (number of Cartesian velocity components used in translating the calculated velocity fields) = 6. Taking F to be that value of (9) determined in the inversions,

$$F = \frac{32.6/2}{615.5/(155-6-2)} = 3.89$$

leads to $P_F = 3\%$. We conclude that the postseismic relaxation effects estimated jointly with uniform afterslip rates are significant at the 97% confidence level.

Another estimate of the relative size of postseismic relaxation can be made by comparing the observed displacement field with the relaxation component obtained on model A (Figure 5). This indicates that the relative size of relaxation is about $(0.15 \text{ cm/yr})/(3 \text{ cm/yr})=5\%$ in the near-source region but up to 100% beyond about one fault length away from the near-source region. This suggests that lower crustal relaxation effects may be easier to identify in future (post-1994) time periods when the shallow afterslip rates have diminished.

For the period 1989-1994, the inversion results obtained above for the various cases show that a somewhat complicated model is required to satisfactorily explain all of the observations. The large component of fault-normal motions requires the large reverse afterslip rates derived here on two fault planes which are essentially the coseismic rupture plane and its shallowly dipping upward extension. Each of these two afterslip planes is correlated in space with background seismicity. Viscoelastic relaxation of the lower crust and possibly the upper mantle are present at low but significant levels in the first 5 years of data. Relatively low afterslip rates in the strike-slip sense are required when viscoelastic relaxation of the lower crust is included in the modeling.

The coseismic slip distributions of both Beroza [1991] and *Arnadottir and Segall* [1994] are shown in Figure 8. We wish to compare our distributed afterslip model with the coseismic slip distribution, and we choose to compare it directly with the slip distribution determined by *Arnadottir and Segall* [1994] in Figure 8b simply because the slip distributions in that paper and the present paper were derived from geodetic data sources. The distributed afterslip rate for model A is superimposed for both the strike-slip and reverse-slip components of plane 1. It is noteworthy that the maximum afterslip rates on plane 1 occur in the southeast part of the coseismic rupture plane, precisely where there is a deficit in coseismic reverse slip. Combined with existing models of the coseismic rupture, our analysis suggests that slip deficits in both the strike-slip and reverse senses existed near the Loma Prieta rupture zone at the time of the 1989 earthquake. This agrees with the inference of a strike-slip deficit at depths greater than about 10 km along the impending Loma Prieta rupture zone remaining after the 1906 San Francisco earthquake [Segall and Lisowski, 1990]. Most of the slip deficit in the strike-slip sense was then accommodated by the 1989 earthquake, but significant stored strain representing compression perpendicular to the San Andreas fault evidently remained both updip and laterally southeast from that part of the 1989 coseismic rupture zone which experienced significant reverse slip.

An alternative to the afterslip model presented here is the fault zone collapse model of *Savage et al.* [1994], which combines fault-zone collapse in the deeper part of the coseismic rupture plane and oblique afterslip along its downdip extension. Since this model fits the horizontal postseismic data well but the vertical postseismic data poorly, we further explored the possibility of fitting the postseismic velocity data with a model of distributed afterslip and fault zone collapse on the entire coseismic rupture plane. Taking the coseismic rupture plane determined in the constrained model of *Williams et al.* [1993], using the same damping parameter μ as used in deriving model A, and ignoring viscoelastic relaxation, we obtain the results shown in Figures 9 and 10 and listed in Table 2 under model H. It is noteworthy that the distribution of total afterslip is nearly anticorrelated with the distribution of fault zone collapse (Figure 9), and the latter is practically uncorrelated with the coseismic reverse slip distribution (Figure 8b), with a correlation coefficient of only 0.025. It should be expected that coseismic slip and fault zone collapse should be highly correlated if the latter is a viable physical process, so that fault zone collapse does not appear to be a significant process in post-Loma Prieta earthquake deformation. As discussed in paper 1, it should be further noted that while the fit of the fault zone collapse model to the horizontal data is satisfactory (Figure 10), the fit of the vertical data is still poor, and the combination of fault zone collapse and distributed afterslip is not sufficient to overcome this deficiency. Despite these arguments, fault zone collapse should not be ruled out as a contributor to the postseismic velocity field because in the above analysis we have assumed constant rates of fault zone collapse over the entire period 1989-1994, whereas the leveling data constrain only vertical motions over the period 1990-1992. Significant fault zone collapse occurring prior to February, 1990 or later than November, 1992 could be invoked to avoid the difficulties associated with fitting the leveling data.

The San Francisco Bay area deformation as represented by repeated GPS and leveling data discussed here is inadequate to resolve the regional viscoelastic stratification. Two quite

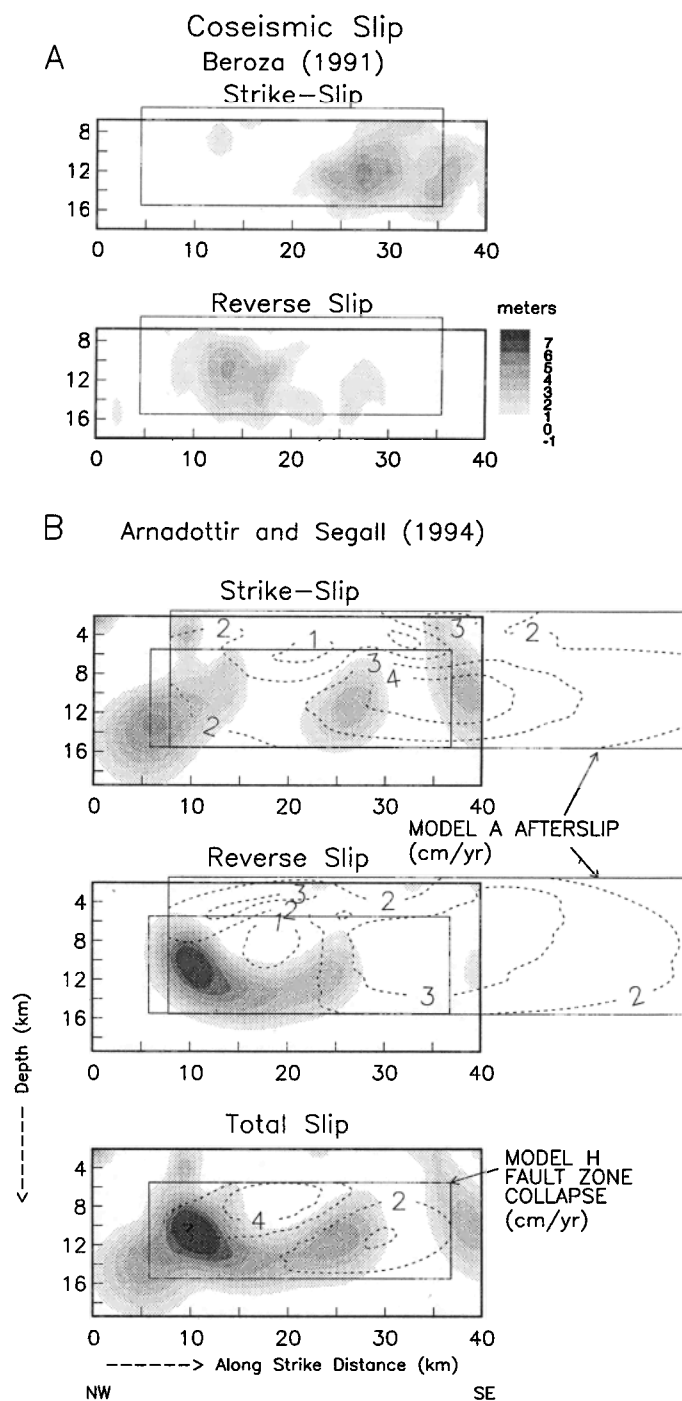


Figure 8. Distribution of coseismic slip (right-lateral strike slip and reverse slip) on rupture planes as determined by (a) *Beroza* [1991] and (b) *Arnadottir and Segall* [1994]. The distributed afterslip rate of plane 1 obtained in model A and distributed fault zone collapse rate obtained in model H are superimposed on the coseismic slip distributions of *Arnadottir and Segall* [1994]. These distributions are all projected onto strike N128° E of the coseismic rupture plane of *Arnadottir and Segall* [1994]. The coseismic rupture plane of *Williams et al.* [1993] projected onto the other coseismic rupture planes along their respective strikes is shown in every case for reference. Greyscale is identical for all subplots.

different rheological models (models A and C) yield the best (and nearly identical) fits of the data involving joint estimation of both distributed afterslip and lower crustal viscoelastic relaxation. In particular, model C takes the lower crust to be a standard linear solid, which can accommodate both ductile flow and long term strength, and this is underlain by a relatively ductile

uppermost mantle. This structure is similar to that obtained by *Pollitz and Sacks* [1992] in northeast Iceland, where low upper mantle viscosities are consistent with the properties of a shallow oceanic asthenosphere [*Davaille and Jaupart*, 1994; *Hirth and Kohlstedt*, 1996]. In a continental region such as California, a weak uppermost mantle would require high temperature,

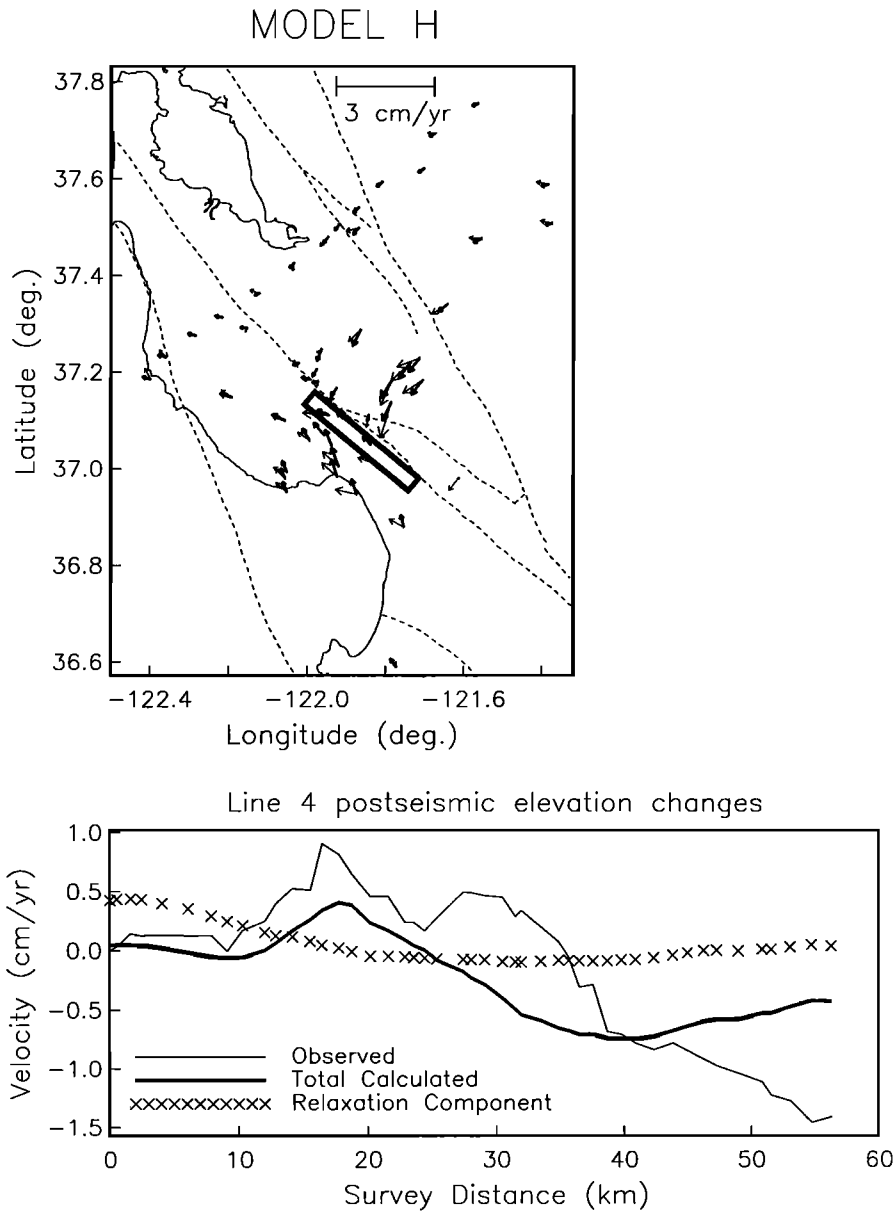


Figure 9. Distribution of afterslip rate (by grey shading) and fault zone collapse (dashed contours) on the coseismic rupture plane (defined by *Williams et al.* [1993] and plotted with heavy lines) for model H, which fits the postseismic velocity data with these processes only. Greyscale is identical for all subplots.

high water content, small grain size, or a combination of these factors [*Kohlstedt et al.*, 1995, and references therein]. A case for elevated temperature can be made from the fact that heat flow along the northern San Andreas fault [*Lachenbruch and Sass*, 1980] is much higher than that measured in regions where a smaller mantle viscosity is inferred (for example, Japan). The breadth of the heat flow anomaly suggests that it is not locally generated by the San Andreas fault but persists over the entire region. It has been suggested from these considerations that the heat flow anomaly has resulted from heat input ~ 20 Myr before Present from asthenospheric upwelling associated with subduction of the Pacific-Farallon ridge crest [*Dickinson and Snyder*, 1979; *Lachenbruch and Sass*, 1980], and shear heating beneath the upper crust generated by interseismic motions [*Thatcher and England*, 1998] may further contribute to the regional heat flow anomaly. Whether or not this fossil heat

input is localized in the crust or upper mantle in the region is unclear, but elevated mantle temperatures extending from the northern Coast Ranges to the southern San Francisco Bay area are suggested by seismic tomography [*Benz et al.*, 1992; *Biasi and Humphries*, 1992; *Pasyanos*, 1996], lending a measure of support to model C.

Although the resolution of the ductile properties of the lower crust and upper mantle obtained here is marginal, the best fitting model suggests nevertheless that a "normal" viscosity lower crust (about 10^{19} Pa s) combined with a much higher mantle viscosity best describes the lithospheric rheology in this region. Such a lithospheric rheology predicts a relatively narrow zone of significant postseismic strain centered on the coseismic rupture area [*Pollitz*, 1992, 1997]. The only independent test of this rheology is the analysis of post-1906 deformation by *Thatcher* [1983], showing high rates of postseismic deformation

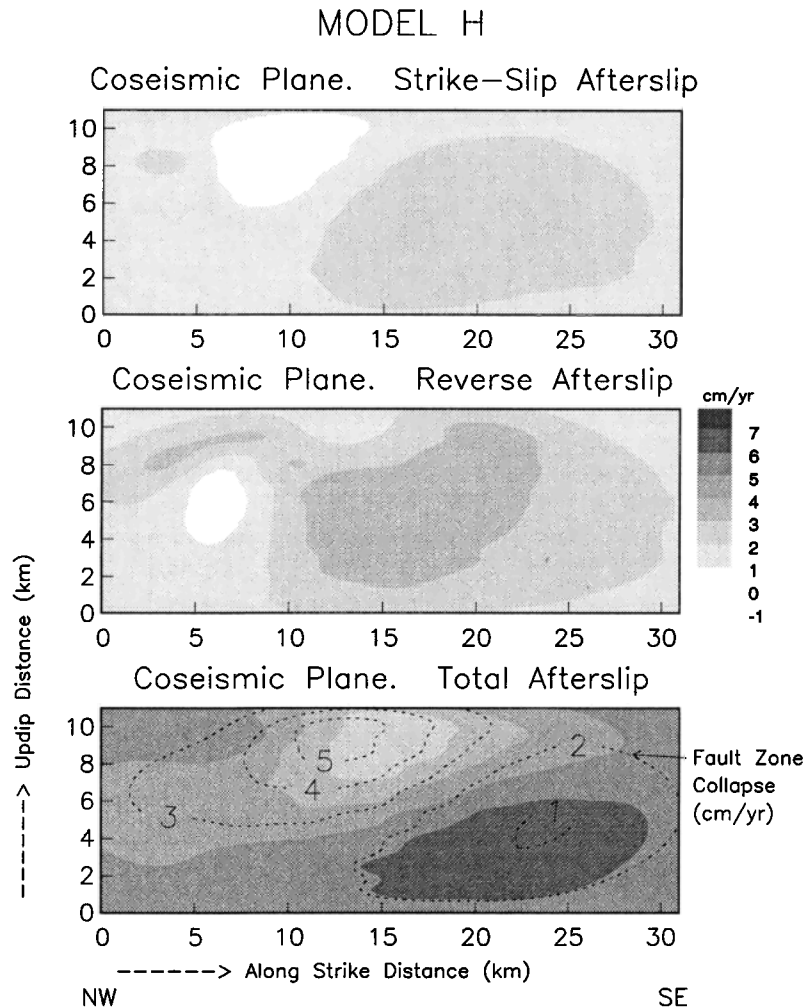


Figure 9. (continued)

over a period of about 30 years within a narrow region centered on the San Andreas fault. According to Thatcher, the post-1906 time-dependent data available near the San Andreas fault can be interpreted equally well in terms of either deep afterslip (localized in the lower crust or deeper) or viscoelastic relaxation of the lower crust with viscosity 3×10^{19} Pa s. If a viscoelastic relaxation mechanism is chosen, however, then the post-1906 observations are consistent with the regional rheology determined here from the post-1989 observations.

Ongoing studies in southern California suggest, as does the present study, that upper crustal afterslip and lower crustal viscoelastic relaxation have been observable processes following recent large earthquakes. The regional deformation following the 1992 Landers earthquake appears to require a combination of afterslip to explain horizontal GPS observations [Savage and Svarc, 1997] and lower crustal relaxation to explain longer wavelength patterns emerging from dominantly vertical Synthetic Aperture Radar (SAR) observations (G. Peltzer, personal communication, 1998). Lower crustal relaxation does not appear to be the dominant process in the short term following the 1994 Northridge earthquake [Donnellan and Lyzenga, 1998]. In the post-Landers and post-Loma Prieta cases, the postseismic evolution appears to exhibit a rapid afterslip phase with a time constant of several weeks (post-Landers [Shen *et al.*, 1994; Yu *et al.*, 1996]) or 1-2 years (post-Loma Prieta

[Savage *et al.*, 1994; Segall and Bürgmann, 1997]). Although several investigators have postulated either upper crustal or lower crustal afterslip for each event [e.g., Savage *et al.*, 1994; Savage and Svarc, 1997; Bürgmann *et al.*, 1997]), the picture which emerges is that the postseismic evolution may generally consist of a rapid afterslip phase superimposed on a more gradual lower crustal/upper mantle viscoelastic relaxation phase.

7. Conclusions

Our analysis of the postseismic velocity pattern in the 5 years following the 1989 Loma Prieta earthquake strongly suggests that a fairly complicated catalogue of physical effects were in operation. Afterslip on predominantly the coseismic rupture plane and its updip extension accompanied by viscoelastic relaxation of the lower crust all play a role in shaping the postseismic velocity field. All of these processes were likely triggered by the stress changes associated with the October 17, 1989 main shock.

Specific conclusions of this study are as follows:

1. The postseismic surface velocity field measured with GPS and repeated leveling in the 5 years following the 1989 Loma Prieta earthquake can not be fit with a model of deep viscoelastic relaxation alone. A model of distributed afterslip on two well defined planes explains a large fraction of the signal

in the data. One of these planes represents the coseismic rupture plane plus its southeast lateral extension, and the other is a shallowly dipping reverse fault located updip from the coseismic rupture plane.

2. Allowance for viscoelastic relaxation of the lower crust yields a significant improvement to the model fit for that class of models involving uniform afterslip plus viscoelastic relaxation.

3. Different candidate models of lower crustal and upper mantle rheology can not be distinguished with the data set analyzed here. A Maxwell viscoelastic lower crust with viscosity of about 10^{19} Pa s underlain by a purely elastic ("strong") mantle and a viscoelastic lower crust (standard linear solid) of slightly greater viscosity underlain by a Maxwell viscoelastic upper mantle with viscosity near 10^{19} Pa s are equally capable of explaining the relaxation signal present in the data.

4. The maximum reverse afterslip rates on the slip-distributed models are 3–5 cm/yr over a 5-year period. Relative to the coseismic slip distribution, the reverse afterslip appears to be concentrated both along the immediate southeast lateral extension and updip of the centers of significant coseismic reverse slip.

5. Possible afterslip far to the southeast of the coseismic rupture zone cannot be constrained with the present data set.

6. Most of the signal in the postseismic velocity field is associated with afterslip on the two principal identified afterslip planes. A small but significant part of the signal appears to be associated with deeper viscoelastic relaxation. More direct detection of a significant viscoelastic relaxation component following the Loma Prieta earthquake should be improved by analysis of more recent GPS data.

Acknowledgments. This work was supported by the Cooperative UC/Los Alamos Research program and a Presidential Young Investigators award to Louise Kellogg. Constructive comments from Yehuda Bock and an anonymous reviewer are gratefully acknowledged.

References

- Abramowitz, M., and I.A. Stegun, *Handbook of Mathematical Functions With Formulas, Graphs, and Mathematical Tables*, 1046 pp., Nat. Bur. of Stand., Washington, 1964.
- Aki, K., Magnitude-frequency relation for small earthquakes: A clue to the origin of f_{\max} of large earthquakes, *J. Geophys. Res.*, *92*, 1349-1355, 1987.
- Amadottir, T., P. Segall, and M. Matthews, Resolving the discrepancy between geodetic and seismic fault models for the 1989 Loma Prieta, California, earthquake, *Bull. Seismol. Soc. Am.*, *82*, 2248-2255, 1992.
- Amadottir, T., and P. Segall, The 1989 Loma Prieta earthquake imaged from inversion of geodetic data, *J. Geophys. Res.*, *99*, 21,835-21,855, 1994.
- Benz, H.M., G. Zandt, and D.H. Oppenheimer, Lithospheric structure of northern California from teleseismic images of the upper mantle, *J. Geophys. Res.*, *97*, 4791-4807, 1992.
- Beroza, G.C., Near-source modeling of the Loma Prieta earthquake: Evidence for heterogeneous slip and implications for earthquake hazard, *Bull. Seismol. Soc. Am.*, *81*, 1603-1621, 1991.
- Bevington, P.R., *Data Reduction and Error Analysis for the Physical Sciences*, 336 pp., McGraw-Hill, New York, 1969.
- Biasi, G.P. and E.D. Humphries, P-wave image of the upper mantle structure of central California and southern Nevada, *Geophys. Res. Lett.*, *19*, 1161-1164, 1992.
- Blümling, P., W.D. Mooney, and W.H.K. Lee, Crustal structure of the southern Calaveras fault zone, central California, from seismic refraction investigations, *Bull. Seismol. Soc. Am.*, *75*, 193-209, 1985.
- Brace, W.F. and D.L. Kohlstedt, Limits on lithospheric stress imposed by laboratory experiments, *J. Geophys. Res.*, *85*, 6248-6252, 1980.
- Bürgmann, R., P. Segall, M. Lisowski, and J. Svarc, Postseismic strain following the 1989 Loma Prieta earthquake from GPS and leveling measurements, *J. Geophys. Res.*, *102*, 4933-4955, 1997.
- Chen, W.-P., and P. Molnar, Focal depths of intracontinental and intra-plate earthquakes and their implications for the thermal and mechanical properties of the lithosphere, *J. Geophys. Res.*, *88*, 4183-4214, 1983.
- Cohen, S.C., A multilayer model of time dependent deformation following an earthquake on a strike-slip fault, *J. Geophys. Res.*, *87*, 5409-5421, 1982.
- Dickinson, W.R., and W.S. Snyder, Geometry of subducted slabs related to San Andreas transform, *J. Geol.*, *87*, 609-627, 1979.
- Davaille, A. and C. Jaupart, Onset of thermal convection in fluids with temperature-dependent viscosity: Application to the oceanic mantle, *J. Geophys. Res.*, *99*, 19853-19866, 1994.
- Dietz, L.D., and W.L. Ellsworth, The October 17, 1989 Loma Prieta, California, earthquake and its aftershocks: Geometry of the sequence from high resolution locations, *Geophys. Res. Lett.*, *17*, 1417-1420, 1990.
- Donnellan, A. and G.A. Lyzenga, GPS observations of fault afterslip and upper crustal deformation following the Northridge earthquake, *J. Geophys. Res.*, *103*, 21285-21297, 1998.
- Foulger, G.R., C.-H. Jahn, G. Seeber, P. Einarsson, B.R. Julian, and K. Heki, Post rifting stress relaxation at the accretionary plate boundary in Iceland measured using the Global Positioning System, *Nature*, *358*, 488-490, 1992.
- Friederich, W. and E. Wielandt, Interpretation of seismic surface waves in regional networks: Joint estimation of wavefield geometry and local phase velocity: Method and numerical tests, *Geophys. J. Int.*, *120*, 731-744, 1995.
- Hirth, G., and D.L. Kohlstedt, Water in the oceanic upper mantle: Implications for rheology, melt extraction and the evolution of the lithosphere, *Earth Planet. Sci. Lett.*, *144*, 93-108, 1996.
- Jachens, R.C., and A. Griscorn, Geologic and geophysical setting of the 1989 Loma Prieta earthquake, California, inferred from magnetic and gravity anomalies, *U.S. Geol. Surv. Prof. Pap.*, in press, 1998.
- Kanamori, H., and K. Satake, Broadband study of the Loma Prieta earthquake, *Geophys. Res. Lett.*, *17*, 1179-1182, 1990.
- Kohlstedt, D.L., B. Evans, and S.J. Mackwell, Strength of the lithosphere: Constraints imposed by laboratory experiments, *J. Geophys. Res.*, *100*, 17587-17602, 1995.
- Lachenbruch, A.H., and J.H. Sass, Heat flow and energetics of the San Andreas fault zone, *J. Geophys. Res.*, *85*, 6185-6222, 1980.
- Langbein, J., and H. Johnson, Correlated errors in geodetic time series: Implications for time-dependent deformation, *J. Geophys. Res.*, *102*, 591-603, 1997.
- Linker, M.F., and J.R. Rice, Models of postseismic deformation and stress transfer associated with the 1989 Loma Prieta earthquake, *U.S. Geol. Surv. Prof. Pap.*, *1550-D*, 253-275, 1997.
- Lisowski, M., W.H. Prescott, J.C. Savage, and M.J. Johnston, Geodetic estimate of coseismic slip during the 1989 Loma Prieta, California, earthquake, *Geophys. Res. Lett.*, *17*, 1437-1440, 1990.
- Marshall, G.A., R.S. Stein, and W. Thatcher, Faulting geometry and slip from co-seismic elevation changes: The October 17, 1989 Loma Prieta, California, earthquake, *Bull. Seismol. Soc. Am.*, *81*, 1660-1693, 1991.
- Olson, J.A., and D.P. Hill, Seismicity in the southern Santa Cruz mountains during the 20-year period before the earthquake, *U.S. Geol. Surv. Prof. Pap.*, *1550-C*, 3-16, 1991.
- Oppenheimer, D.H., W.H. Bakun, and A.G. Lindh, Slip partitioning of the Calaveras fault, California, and prospects for future earthquakes, *J. Geophys. Res.*, *95*, 8483-8498, 1990.
- Pasyanos, M.E., Regional moment tensors and the structure of the crust in central and northern California, thesis, Univ. of Calif., Berkeley, 1996.
- Pollitz, F.F., Postseismic relaxation theory on the spherical Earth, *Bull. Seismol. Soc. Am.*, *82*, 422-453, 1992.

- Pollitz, F.F., Coseismic deformation from earthquake faulting on a layered spherical Earth, *Geophys. J. Int.*, *125*, 1-14, 1996.
- Pollitz, F.F., Gravitational-viscoelastic postseismic relaxation of a layered spherical Earth, *J. Geophys. Res.*, *102*, 17921-17941, 1997.
- Pollitz, F.F., and I.S. Sacks, Modeling of postseismic relaxation following the great 1857 earthquake, southern California, *Bull. Seis. Soc. Am.*, *82*, 454-480, 1992.
- Pollitz, F.F., and I.S. Sacks, Viscosity structure beneath northeast Iceland, *J. Geophys. Res.*, *101*, 17771-17793, 1996.
- Romanowicz, B., and H. Lyon-Caen, The Loma Prieta earthquake of October 18, 1989: Results of teleseismic mantle and body wave inversion, *Geophys. Res. Lett.*, *17*, 1191-1194, 1990.
- Ruff, L.J., and B.W. Tichelaar, Moment tensor rate functions for the 1989 Loma Prieta earthquake, *Geophys. Res. Lett.*, *17*, 1187-1190, 1990.
- Rydelek, P.A., and I.S. Sacks, Asthenospheric viscosity inferred from correlated land-sea earthquakes in north-east Japan, *Nature*, *336*, 234-237, 1988.
- Rydelek, P.A., and I.S. Sacks, Asthenospheric viscosity and stress diffusion: A mechanism to explain correlated earthquakes and surface deformations in northeast Japan, *Geophys. J. Int.*, *100*, 39-58, 1990.
- Savage, J.C., Strain accumulation in the western United States, *Annu. Rev. Earth Planet Sci. Lett.*, *11*, 11-43, 1983.
- Savage, J.C., Equivalent strike-slip earthquake cycles in half-space and lithosphere-asthenosphere Earth models, *J. Geophys. Res.*, *95*, 4873-4879, 1990.
- Savage, J.C., and W.H. Prescott, Asthenospheric readjustment and the earthquake cycle, *J. Geophys. Res.*, *83*, 3369-3376, 1978.
- Savage, J.C., and J.L. Svarc, Postseismic deformation associated with the 1992 $M_w = 7.3$ Landers earthquake, southern California, *J. Geophys. Res.*, *102*, 7565-7577, 1997.
- Savage, J.C., M. Lisowski, and J.L. Svarc, Postseismic deformation following the 1989 ($M=7.1$) Loma Prieta, California, earthquake, *J. Geophys. Res.*, *99*, 13757-13765, 1994.
- Scholz, C.H., and T. Kato, The behavior of a convergent plate boundary: Crustal deformation in the South Kanto District, Japan, *J. Geophys. Res.*, *83*, 783-797, 1978.
- Seeber, L., and J.G. Armbruster, fault kinematics in the 1989 Loma Prieta rupture zone during 20 years before that event, *Geophys. Res. Lett.*, *17*, 1425-1428, 1990.
- Segall, P. and R. Bürgmann, Triggered time-dependent slip following the 1989 Loma Prieta earthquake, *Eos Trans. AGU*, *78* (46), Fall Meeting Suppl., F165, 1997.
- Segall, P. and M. Lisowski, Surface displacements in the 1906 San Francisco and 1989 Loma Prieta earthquakes, *Science*, *250*, 1241-1244, 1990.
- Shen, Z.K., D.D. Jackson, Y. Feng, M. Cline, M. Kim, P. Fang, and Y. Bock, Postseismic deformation following the Landers earthquake, California, 28 June 1992, *Bull. Seismol. Soc. Am.*, *84*, 780-791, 1994.
- Snay, R.A., H.C. Neugebauer, and W.H. Prescott, Horizontal deformation associated with the 1989 Loma Prieta earthquake, *Bull. Seismol. Soc. Am.*, *81*, 1647-1659, 1991.
- Tabei, T., Crustal movements in the inner zone of southwest Japan associated with stress relaxation after major earthquakes, *J. Phys. Earth*, *37*, 101-131, 1989.
- Thatcher, W., Strain release mechanism of the 1906 San Francisco earthquake, *Science*, *184*, 1283-1285, 1974.
- Thatcher, W., Nonlinear strain buildup and the earthquake cycle on the San Andreas fault, *J. Geophys. Res.*, *88*, 5893-5902, 1983.
- Thatcher, W., and P.C. England, Ductile shear zones beneath strike-slip faults: Implications for the thermomechanics of the San Andreas fault, *J. Geophys. Res.*, *103*, 891-905, 1998.
- Thatcher, W., T. Matsuda, T. Kato, and J.B. Rundle, Lithospheric loading by the 1896 Riku-u earthquake, northern Japan: Implications for plate flexure and asthenospheric rheology, *J. Geophys. Res.*, *85*, 6429-6435, 1980.
- Wald, D., D.V. Helmberger, and T.H. Heaton, Rupture model of the 1989 Loma Prieta earthquake from the inversion of strong-motion and broadband teleseismic data, *Bull. Seismol. Soc. Am.*, *81*, 1540-1572, 1991.
- Wallace, T.C., A. Velašco, J. Zhang, and T. Lay, A broadband seismological investigation of the 1989 Loma Prieta, California, earthquake: Evidence for deep slow slip?, *Bull. Seismol. Soc. Am.*, *81*, 1622-1646, 1991.
- Williams, C.R., T. Armadottir, and P. Segall, Coseismic deformation and dislocation models of the 1989 Loma Prieta earthquake derived from Global Positioning System measurements, *J. Geophys. Res.*, *98*, 4567-4578, 1993.
- Wyatt, F.K., Displacement of surface monuments: Vertical motion, *J. Geophys. Res.*, *94*, 1655-1664, 1989.
- Yu, T.-T., J.B. Rundle, and J. Fernandez, Surface deformation due to a strike-slip fault in an elastic gravitational layer overlying a viscoelastic gravitational half-space, *J. Geophys. Res.*, *101*, 3199-3214, 1996.

R Bürgmann, Department of Geology and Geophysics, University of California, Berkeley, CA 94720.

F. F. Pollitz, Department of Geology, University of California, Davis, CA 95616. (email: pollitz@geology.ucdavis.edu)

P. Segall, Department of Geophysics, Stanford University, Stanford, CA 94305. (email: segall@halape.stanford.edu)

(Received September 16, 1997; revised March 6, 1998; accepted May 6, 1998.)